

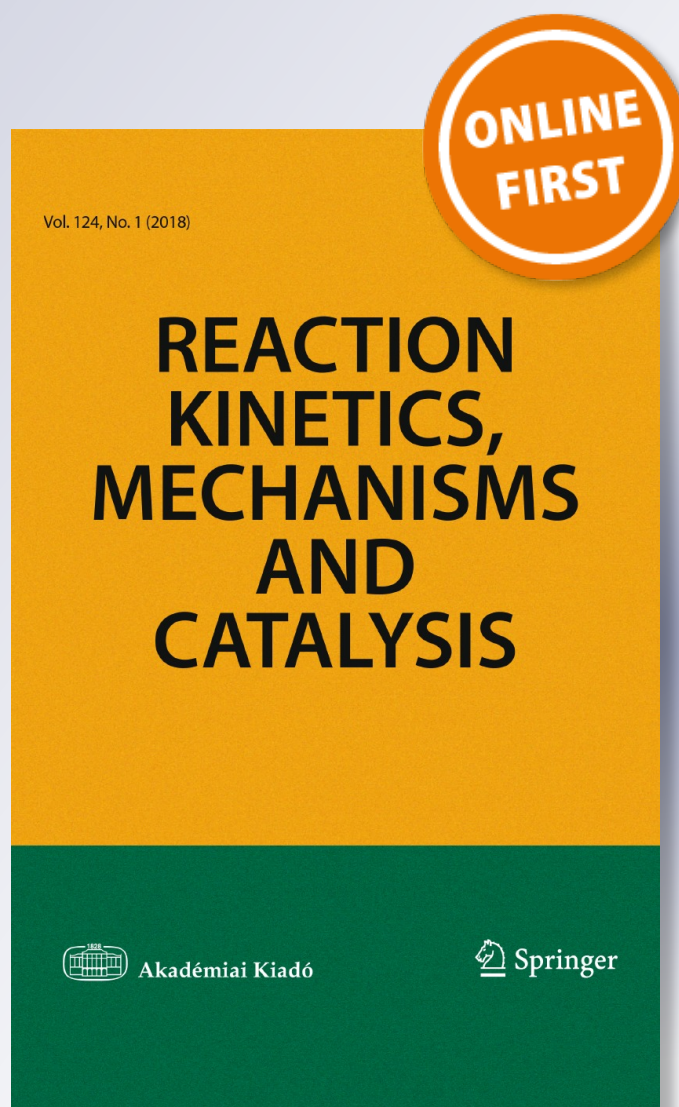
*Optimization and modeling of CO<sub>2</sub> photoconversion using a response surface methodology with porphyrin-based metal organic framework*

**Nasrin Sadeghi, Shahram Sharifnia & Trong-On DO**

**Reaction Kinetics, Mechanisms and Catalysis**

ISSN 1878-5190

Reac Kinet Mech Cat  
DOI 10.1007/s11144-018-1407-z



**Your article is protected by copyright and all rights are held exclusively by Akadémiai Kiadó, Budapest, Hungary. This e-offprint is for personal use only and shall not be self-archived in electronic repositories. If you wish to self-archive your article, please use the accepted manuscript version for posting on your own website. You may further deposit the accepted manuscript version in any repository, provided it is only made publicly available 12 months after official publication or later and provided acknowledgement is given to the original source of publication and a link is inserted to the published article on Springer's website. The link must be accompanied by the following text: "The final publication is available at [link.springer.com](http://link.springer.com)".**

# Optimization and modeling of CO<sub>2</sub> photoconversion using a response surface methodology with porphyrin-based metal organic framework

Nasrin Sadeghi<sup>1</sup> · Shahram Sharifnia<sup>1</sup> · Trong-On DO<sup>2</sup>

Received: 29 November 2017 / Accepted: 13 April 2018  
© Akadémiai Kiadó, Budapest, Hungary 2018

**Abstract** In the current study, porphyrin-based metal organic framework (M(metal)/PMOF) was used to photoreduction conversion of CO<sub>2</sub> under UV/Visible light irradiation. The metal and linker selection in the M/PMOF synthesis influences its structure and properties. In this regards, M/PMOFs were prepared using three different metals of Zn, Al, and Co. The prepared photocatalysts were characterized by powder X-ray diffraction (XRD), N<sub>2</sub> adsorption BET surface area, scanning electron microscopy (SEM), Energy dispersive X-ray spectrometer (EDX), Fourier transform infrared (FTIR) and UV–Vis spectroscopy. Also, the photoluminescent properties and photoreactor tests, for these three photocatalysts were investigated. The obtained results demonstrated that Al/PMOF has high CO<sub>2</sub> photoreduction conversion, 4.3%. The operating conditions were optimized to find the best conditions which are lead to high CO<sub>2</sub> photoreduction conversion over Al/PMOF. For this purpose, the experiments were conducted based on central composite design (CCD) and analyzed using response surface methodology (RSM). The ANOVA analysis revealed that the maximum photoreduction conversion of CO<sub>2</sub>, as 10.63%, can be obtained at the optimum conditions (catalyst amount of 297.24 mg, total feed pressure of 1.4 atm and methanol as sacrificial agent). Finally, a verification experiment was performed and results confirmed the validity and adequacy of the predicted model for simulating the CO<sub>2</sub> photocatalytic conversion.

**Electronic supplementary material** The online version of this article (<https://doi.org/10.1007/s11144-018-1407-z>) contains supplementary material, which is available to authorized users.

✉ Shahram Sharifnia  
sharif@razi.ac.ir

<sup>1</sup> Catalyst Research Center, Chemical Engineering Department, Razi University, Kermanshah, Iran

<sup>2</sup> Department of Chemical Engineering, Laval University, Quebec G1V0A8, Canada

**Keywords** Photocatalyst · Metal organic framework · Optimization · Response surface methodology · CO<sub>2</sub> photoreduction

## Introduction

Carbon dioxide (CO<sub>2</sub>) as a primary greenhouse gas plays a significant role in global warming. In this respect, there have been a variety of programs of policy and action in relation to the environment and among them CO<sub>2</sub> photoreduction process is a popular technology used for reducing CO<sub>2</sub> in last decades, however, few reports dealing with the application of statistical design of experiments towards the operational optimization of this process. The photocatalytic reduction of CO<sub>2</sub> is a complex process and involved complicated chain reactions, which generally require a number of assumptions to solve the equations derived on the basis of physical and concepts [1–3]. In the CO<sub>2</sub> photoreduction process, possible variables that affect the photocatalytic reduction efficiency could be initial CO<sub>2</sub> pressure, catalyst amount and/or characteristics, illumination time, light irradiance (power and/or intensity), temperature and electron acceptors [4, 5]. The traditional “trial-and-error” and one-factor-at-a-time (OFAT) optimization approaches can be applied to optimize CO<sub>2</sub> photoreduction process [2, 4]. The major disadvantage of OFAT approach is that it does not include interactive effects among the variables and, finally, it does not describe the complete effects of the parameters on the process [6, 7]. Another disadvantage is a large number of experiments needed which means require additional time and also additional expense due to reagent costs [2, 8, 9]. Another less frequently used approach is artificial neural networks (ANNs). The neural networks behave as ‘black boxes’ and can be simply used to estimate various parameters as a function of different variables [10–13]. The most significant advantages of these modeling techniques are the computational efficiency, the possibility to apply it on complex non-linear processes, the ease of manipulation [2, 14, 15]. Nevertheless, the disadvantages of the ANNs approach are the selection of regression variables, the necessity of obtaining a perfect neural network model based on experimental or operational history data [2, 13, 14, 16]. In general, the main aim of optimization is to improve the systems performance and to enhance the yield of the processes while not increasing the cost [6, 17]. In this respect, the number of experiments has a crucial role in operational and capital costs. More experiments require more material, more analysis and spent more time [18].

In order to overcome these problems and optimize all of the parameters, the statistical experimental design was applied by response surface methodology (RSM) [19, 20]. RSM is an efficient mathematical model for the optimization of a multivariable system with fewer experimental trials [21–23]. For instance, the central composite design (CCD), an experimental design, was used by RSM to fit a model by least squares technique [24, 25]. Adequacy of the suggested model is then evaluated using the diagnostic checking tests provided by analysis of variance (ANOVA). The response surface plots can be applied to consider the surfaces and locate the optimum. In recent years, RSM is commonly used to evaluate the results

and operations efficiency even in many industrial processes [26–30]. In 2016, Mosleh et al. [31] synthesized  $\text{BiPO}_4/\text{Bi}_2\text{S}_3$ -HKUST-1-MOF and applied in a catalytic rotating packed bed reactor for photocatalytic degradation of toluidine blue (TB) and auramine-O (AO). CCD was applied to optimize operational parameters: irradiation time, pH, photocatalyst dosage, rotational speed, solution flow rate, aeration flow rate and TB and AO concentration. Totally 52 experiments were performed to find the optimum values for each parameter. At optimum condition, the photocatalytic degradation percentages of TB and AO were 99.37 and 98.44%, respectively. In another study, Mosleh et al. [32] used  $\text{Ag}_3\text{PO}_4/\text{Bi}_2\text{S}_3$ -HKUST-1-MOF to sonophotocatalytic degradation of trypan blue (TB) and vesuvine (VS). The effect of operational parameters including the initial TB and VS concentration, flow rate, irradiation and sonication time, pH and photocatalyst dosage were investigated and optimized using CCD combined with desirability function (DF). Under the optimized conditions, the hybrid system was found to have higher efficiency compared with sum of the individual processes. According to our knowledge, no prior work regarding optimizing the operational parameters to obtain high  $\text{CO}_2$  photoreduction conversion over MOF has been reported to date, which is important for scale-up and commercialization purposes have been made.

This present study follows on from our previous work [1]. Previously we reported Zn/PMOF to photoreduction of  $\text{CO}_2$  in the presence of the  $\text{H}_2\text{O}$  vapor as an electron donor under UV/Visible light. Forasmuch as the choice of metal and linker dictates the structure and therefore properties of MOFs, it can be easy to construct MOFs with desirable properties for specific application in  $\text{CO}_2$  reduction [33]. In this respect, different metals are chosen to prepare M/PMOF [M: metal (Al and Co)] and are used for photocatalytic reduction of  $\text{CO}_2$  under same reaction conditions of our previous study [1]. The results are compared and the best photocatalyst with high  $\text{CO}_2$  photoreduction conversion is chosen. Thereafter, the effects of several operating parameters (amount of the catalyst, total pressure of feed and sacrificial agent) are investigated. For this purpose, the central composite design (CCD) along with RSM has been applied to the modeling and optimization of  $\text{CO}_2$  photoreduction conversion. Finally, the best operating condition which is lead to high  $\text{CO}_2$  photoreduction conversion is obtained.

## Experimental

### Materials

Pyrrrole and 4-carboxybenzaldehyde were purchased from the Aldrich Chemical Co.  $\text{CH}_3\text{Cl}$ , acetone, methanol, Acetonitrile (MeCN), propionic acid, DMF,  $\text{Co}(\text{NO}_3)_2 \cdot 6\text{H}_2\text{O}$  and  $\text{Al}(\text{NO}_3)_3 \cdot 9\text{H}_2\text{O}$  were supplied by Merck. All chemicals were used as received without further purification. The  $\text{CO}_2$  gas with 99% purity was used as the feed gas. The deionized water was used to prepare the catalyst.

## Preparation of catalyst

Tetrakis (4-carboxy phenyl) porphyrin (TCPP) was synthesized according to the method provided in our previous paper [1]. To prepare the catalyst, 0.39 g TCPP was introduced into 0.13 L DMF and dissolved on a stirring hot plate. The reaction was allowed to proceed for 20 min and then followed by the addition of 2.017 mmol metal (0.75 g  $\text{Al}(\text{NO}_3)_3 \cdot 9\text{H}_2\text{O}$  and 0.6 g  $\text{Co}(\text{NO}_3)_2 \cdot 6\text{H}_2\text{O}$ ). The solution was allowed to react on the stirring hot plate for about 30 min and then transferred into a 250 mL Teflon-lined autoclave and heated at 180 °C for 24 h. After the solution was cooled down to room temperature, the solid was centrifuged and washed 3 times with deionized water. Finally, the obtained powder was dried at 60 °C.

## Photocatalyst characterization

Powder XRD patterns were recorded on a Bruker SMART APEXII X-ray diffractometer equipped with a  $\text{CuK}_\alpha$  radiation source ( $\lambda=1.5418 \text{ \AA}$ ).  $\text{N}_2$  adsorption–desorption isotherms were obtained at 77 K using Quantachrome Autosorb-1 MP analyzer. Before the measurements, the samples were outgassed under vacuum for 6 h at 150 °C. Scanning electron microscopic (SEM) images were captured using a JOEL JEM 1230 operated at 120 kV. The elemental composition of the catalyst was analyzed by energy dispersive X-ray spectrometer (EDX). The Fourier transform infrared spectroscopy (FTIR) was recorded with an ALPHA (Bruker, Germany) FTIR spectrophotometer. Samples of 1–2 mg were mixed with 100 mg KBr and pressed into translucent disks at room temperature. All spectra were taken in the range 400–4000  $\text{cm}^{-1}$  at a resolution of 4  $\text{cm}^{-1}$ . UV–Vis spectra were recorded on a Cary 100 Scan UV–Vis spectrophotometer (Varian, USA) at room temperature (23–25 °C). The photoluminescence spectra of samples were performed with a JASCO spectrophotometer Model FP-6200 equipped with a thermostat bath, using a 1.0 cm quartz cell. The diffuse reflectance UV–Vis spectra of the Al/PMOF and Co/PMOF powders were obtained by using Avantes spectrometer (Avaspec-2048-TEC) with a reflectance sphere in the range, 300–900 nm.

## Photoreactor system

The photoreactor system and the light source were selected similar to our previous study [1]. The  $\text{CO}_2$  photoreduction was investigated in a batch reactor in the gaseous phase. The photoreactor was made from stainless steel and built in the laboratory. The effective volume of the reaction system was about 1 L. The photocatalyst powders were ground to obtain fine particles and then distributed at the bottom of the reactor. A 300 W high-pressure mercury ( $200 < \lambda < 800$ ) was placed in the center of the reactor to direct irradiation on the catalyst surface. At the next step, the reactor was filled with pure  $\text{CO}_2$  with 120 mL/min flow rate and then vacuumed several times to ensure all the impurities and trapped air were completely removed and then it was filled with high purity  $\text{CO}_2$  with 120 mL/min flow rate as feed gas to 1.4, 2.7, 4.1 atm (20, 40, 60 psia) of absolute total pressure. Different amount of

sacrificial agent (0.6, 2.96 and 4.52 mL for H<sub>2</sub>O, MeCN, and methanol) was subsequently injected into the reactor as a reducer. Before starting the reaction, the gas feed concentration was analyzed by using an on-line commercial gas chromatograph GC-CGCA-1 apparatus. Then the reactor was illuminated for 4 h continuously. During the reaction, the temperature was kept at 100 °C by a jacket around the reactor equipped with a circulating cold water bath. After 4 h irradiation, the products were analyzed by using on-line GC. Decreasing (conversion (%)) of CO<sub>2</sub> was used for evaluation the efficiency of photocatalytic activity (Eq. (1)):

$$\text{Conversion of CO}_2 (\%) = \frac{(\text{Mole of CO}_2^i - \text{Mole of CO}_2)}{\text{Mole of CO}_2^i} \times 100 \quad (1)$$

where CO<sub>2</sub><sup>i</sup> and CO<sub>2</sub> are the concentration of CO<sub>2</sub> at the beginning and the end of the reaction time, respectively.

### Experimental design and optimization by RSM

In this study, central composite design (CCD), which is widely used form of RSM, was employed to optimize operating parameters that maximize the CO<sub>2</sub> photoreduction conversion. For this purpose, Design Expert software was applied. The RSM fundamental assumptions and more detailed information have been described elsewhere [4, 9]. Forasmuch as there has not been a great deal of study done on the pressure effects on the MOF's behavior [34], the effect of the pressure on the CO<sub>2</sub> photoreduction process is studied. The studied photoreactor was tested to operate at 6 atm, higher pressure is possible, however, it was not tested and safe. So, optimization was done at 1.4, 2.7 and 4.1 atm, which are available and safe. On the other hand, electron donor can effect the products yield. Studies [35, 36] were carried out to investigate the effects of the electron donors on the CO<sub>2</sub> photoreduction over different MOFs. With these in mind, different electron donors (methanol where is accessible, H<sub>2</sub>O that is safe, non-toxic and extensively available and MeCN that is commonly used in CO<sub>2</sub> photoreduction over MOFs) were selected as effective parameters. On the other hand, catalyst amount is one of the main parameters that affected the CO<sub>2</sub> reduction but from the economic viewpoint applying more catalyst is not affordable. Consequently, 100, 200, 300 mg catalyst was applied for optimization in order to save money. The experimental ranges and levels of the independent variables for photoreduction of CO<sub>2</sub> are given in Table 1.

**Table 1** Experimental ranges and levels of the independent variables

Variables	Ranges and levels		
	- 1	0	+ 1
Amount of catalyst, mg ( $X_1$ )	100	200	300
Total pressure of feed, atm ( $X_2$ )*	1.4	2.7	4.1
Sacrificial agent ( $X_3$ )	H <sub>2</sub> O	MeCN	Methanol

\*Total pressure of feed ( $X_2$ ): 20, 40 and 60 psia

Totally 39 experiments with three main factors were performed. The complete experimental design matrix and the responses based on experiments proposed by CCD for photoreduction of CO<sub>2</sub> are given in Table 2. The following second-order (quadratic) polynomial response equation was used to correlate the dependent and independent variables:

$$Y(\%) = b_0 + \sum_i b_i x_i + \sum_i \sum_j b_{ij} x_i x_j + \sum_i b_{ii} x_i^2 \quad (2)$$

Where Y is the response variable of conversion efficiency,  $b_0$  is the constant coefficient,  $b_i, b_{ii}$  and  $b_{ij}$  present the regression coefficients for linear, quadratic effects and the coefficients of the interaction parameters, respectively, and  $x_i$  are the independent variables studied.

Analysis of variance (ANOVA) for final predictive equation was used to obtain the interaction between the process variables and the responses. The quality of the fit second-order polynomial equation was expressed by the correlation coefficient ( $R^2$ ) and its statistical significance was determined by the Fisher's F-test in the same program. The model's terms were evaluated according to p-value (probability). Three-dimensional plots and their respective contour plots were obtained for CO<sub>2</sub> photoreduction conversion based on the effect of the three independent variables (catalyst amount, pressure and sacrificial agent) at three levels. Moreover, the optimum region was recognized based on the main parameters in the desirability plot.

## Results and discussion

### Catalyst characterization

XRD analysis was used to investigate the crystal structure of the as-prepared samples. As shown in Fig. 1a, all diffraction peaks for Al/PMOF are indexed to an orthorhombic structure with *Cmmm* symmetry. The cell parameters have been known with  $a = 31.978 \text{ \AA}$ ,  $b = 6.5812 \text{ \AA}$  and  $c = 16.862 \text{ \AA}$ . As a result, the main peaks obtained at  $2\theta = 7.43^\circ$  and  $13.67^\circ$  could be indexed as the (201) and (110) reflections, respectively. In Al/PMOF, each oxygen in the carboxylate group is coordinated with one Al<sup>3+</sup>, the aluminum coordination consists of four carboxylate-derived oxygen atoms in the equatorial plane and two  $\mu_2$  axial OH<sup>-</sup> bridging adjacent Al<sup>3+</sup> centers to form an infinite Al(OH)O<sub>4</sub> chain which is a common motif for M<sup>3+</sup> frameworks with carboxylate ligands (Fig. 1b) [37, 38]. According to all diffraction peaks for Al/PMOF and Co/PMOF no impurity peaks are observed, Fig. 1a. The relatively strong diffraction intensity demonstrates good crystallinity of both MOF structures.

Fig. 2 demonstrates the nitrogen adsorption–desorption isotherms measured at liquid nitrogen temperature. Both Al/POMF and Co/PMOF exhibit a typical II N<sub>2</sub> adsorption isotherm which is observed in nanoporous or macropores materials or open voids [38]. The BET surface areas were 1142 and 957 cm<sup>2</sup>/g for Al/PMOF and

**Table 2** Experimental design matrix and experimental results with predicted values

Run	Point type	Independent variables			Photoconversion (%)	
		Catalyst amount (mg)	Pressure (atm)	Sacrificial agent	Observed	Predicted
1	Axial	200	1.4	MeCN	9.70	10.10
2	Axial	200	1.4	Methanol	10.50	10.15
3	Center	200	2.7	MeCN	6.30	6.17
4	Fact	300	4.1	MeCN	1.20	1.40
5	Axial	300	2.7	MeCN	6.30	5.97
6	Axial	200	4.1	MeCN	2.05	2.23
7	Fact	100	1.4	MeCN	8.60	8.59
8	Fact	100	4.1	Methanol	3.90	2.71
9	Center	200	2.7	H <sub>2</sub> O	5.20	4.93
10	Fact	100	1.4	Methanol	9.40	8.64
11	Axial	200	4.1	Methanol	3.00	2.86
12	Center	200	2.7	MeCN	6.80	6.17
13	Center	200	2.7	H <sub>2</sub> O	6.10	4.93
14	Axial	100	2.7	Methanol	5.10	5.67
15	Fact	100	4.1	H <sub>2</sub> O	5.09	5.44
16	Fact	300	4.1	H <sub>2</sub> O	4.10	4.71
17	Axial	100	2.7	H <sub>2</sub> O	3.97	4.11
18	Fact	300	1.4	H <sub>2</sub> O	4.30	4.79
19	Axial	100	2.7	MeCN	4.64	5.34
20	Center	200	2.7	Methanol	6.37	6.50
21	Center	200	2.7	H <sub>2</sub> O	4.60	4.93
22	Center	200	2.7	Methanol	5.30	6.50
23	Fact	300	1.4	MeCN	10.35	10.58
24	Axial	300	2.7	H <sub>2</sub> O	5.40	4.74
25	Center	200	2.7	MeCN	7.27	6.16
26	Fact	100	1.4	H <sub>2</sub> O	2.88	2.78
27	Center	200	2.7	Methanol	6.20	6.50
28	Center	200	2.7	H <sub>2</sub> O	5.04	4.93
29	Fact	100	4.1	MeCN	1.80	2.08
30	Center	200	2.7	Methanol	5.90	6.50
31	Axial	200	1.4	H <sub>2</sub> O	3.80	4.28
32	Axial	200	4.1	H <sub>2</sub> O	5.70	5.59
33	Fact	300	4.1	Methanol	2.17	1.99
34	Fact	300	1.4	Methanol	11.02	10.62
35	Center	200	2.7	H <sub>2</sub> O	4.92	4.93
36	Center	200	2.7	Methanol	6.40	6.50
37	Center	200	2.7	MeCN	6.00	6.16
38	Axial	300	2.7	Methanol	6.20	6.31
39	Center	200	2.7	MeCN	6.03	6.16

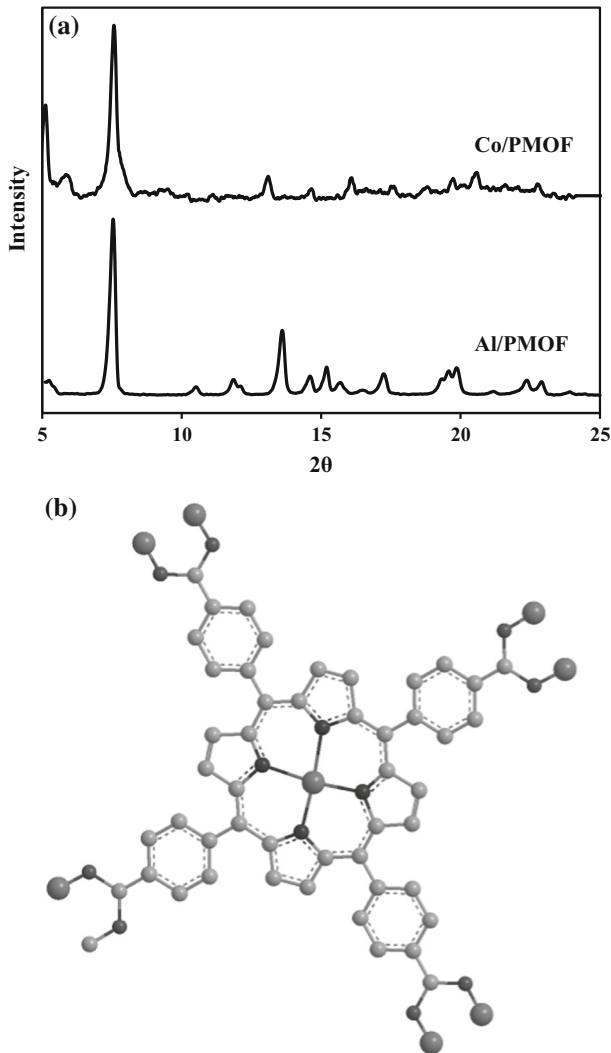


**Fig. 1** **a** XRD patterns of Al/PMOF and Co/PMOF, **b** structure of Al/PMOF. Atoms are colored as follows: dark grey Al, light grey C, dark black N, and light black O

Co/POMF, respectively. The pore volume is 0.606 and 0.348  $\text{cm}^3/\text{g}$  for Al/PMOF and Co/PMOF, respectively.

The morphology of the Al/PMOF and Co/PMOF were examined by SEM. As can be seen in Fig. S1 (supplementary material), the both Al/PMOF and Co/PMOF are composed by nanoplates. EDX analyses were done and confirmed the presence of the Al in Al/PMOF and Co in Co/PMOF structures. In Fig. S2 (supplementary material), the EDX patterns show a clear signal of the Al and Co which indicate Al and Co were successfully incorporated into the Al/PMOF and Co/PMOF frameworks, respectively.

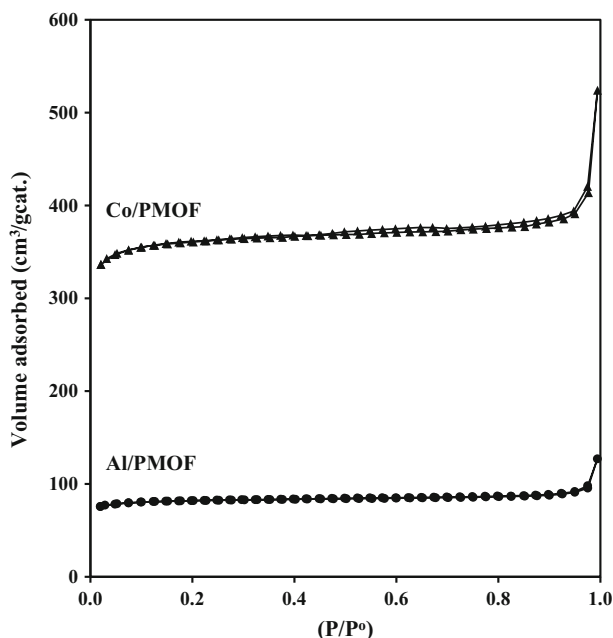


**Fig. 2**  $N_2$  adsorption–desorption isotherms of Al/PMOF and Co/PMOF

The FTIR spectra of TCPP, Co/POMF, and Al/PMOF were shown in Fig. S3 (supplementary material). The typical symmetric and asymmetric stretching bands in the range of the  $700\text{--}1700\text{ cm}^{-1}$  are assigned to the pyrrole ring of  $\nu$  (N–H), (C–H), (C=C) and (C=N) of TCPP ligand. The band appeared about  $3400\text{ cm}^{-1}$  in all three structures is related to the OH vibration of adsorbed water. The FTIR spectra show bands at  $1715$  and  $1179\text{ cm}^{-1}$  which are due to  $\nu$  (C=O) stretch and  $\nu$  (C–O) stretch of the carboxylic acid groups, respectively. The band appearing at  $1500\text{ cm}^{-1}$  is assigned to the  $\nu$  (C=C) stretching vibration in pyrrole ring. It is noticeable that the N–H vibration at  $962\text{ cm}^{-1}$  is disappeared and the new peak at  $1008$  and  $1002\text{ cm}^{-1}$  is appeared in the FTIR spectra of Co/POMF and Al/PMOF, respectively. It is due to the replacement of hydrogen by metal cation [1, 39–42].

The UV–Vis spectra of TCPP, Co/PMOF, and Al/PMOF are demonstrated in the Fig. 3. A typical strong Soret band with  $\lambda_{\text{max}}$  at 418, 424 and 420 nm is shown for TCPP, Co/PMOF, and Al/PMOF, respectively. Due to the metal (Co, Al) insertion in the TCPP structure, a slight shift in the soret band is observed. Furthermore, two weak split Q bands with  $\lambda_{\text{max}}$  at 515 and 553 nm can see for TCPP, respectively. Similar results were reported in the previous studies [37, 39]. The diffuse reflectance UV–Vis spectra of the Al/PMOF and Co/PMOF powders were measured to calculate the band gap energy. Band gap energy was estimated through Tauc relation:

$$(\alpha h\nu)^n = B(h\nu - E_g) \quad (3)$$

where  $h\nu$  is the photon energy,  $\alpha$  is the absorption coefficient, B is a proportionality

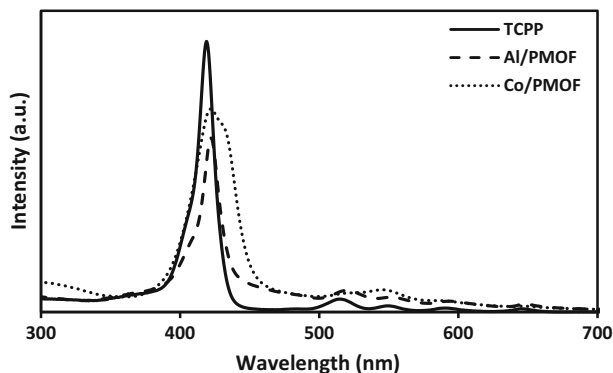


**Fig. 3** UV-Vis spectra of TCPP, Al/PMOF and Co/PMOF in DMF solution

constant,  $E_g$  is the band gap energy, and the exponent  $n$  is a value that depends on the nature of the transition (2 for a direct allowed transition,  $2/3$  for direct forbidden transition and  $1/2$  for indirect allowed transition). MOFs display direct band transition, therefore  $n=2$  [43, 44]. From Tauc plots, Fig. S4 (a) and (b) (supplementary material), the band gaps of Co/PMOF and Al/PMOF are estimated to be 1.92 and 1.89 eV, respectively.

### Photoreactor tests

One of the purposes of the current study was to determine the best M/PMOF with desirable properties in  $\text{CO}_2$  photoreduction process. In this respect, the photoluminescent properties and photoreactor tests of the three photocatalysts, Zn/PMOF [1], Al/PMOF and Co/PMOF, were investigated.

The photoluminescent properties of Zn/PMOF, Al/PMOF, and Co/PMOF were investigated with an excitation wavelength 420 nm. The emission peaks of photocatalysts are illustrated in Fig. 4. Zn/PMOF exhibits an intense emission between 600 and 730 nm with  $\lambda_{max}$  at 647 nm. The photoluminescent of Co/PMOF was slightly quenched. Also, the emission intensity of Al/PMOF was quenched by ca. 70%, indicating that lifetime of photogenerated charge carriers in Al/PMOF is longer than those of Zn/PMOF and Co/PMOF. In other words, it implies that the photogenerated charge carriers can be separated efficiently due to the TCPP excited electron transferring to the conduction band of metal, the mechanism of  $\text{CO}_2$  photoreduction over M/PMOF discussed in our previous work [1]. Also, this behavior can be validated by photoreactor tests illustrated in Fig. 5.

It should be noted that as the different sacrificial agents, such as  $\text{H}_2\text{O}$ , methanol and MeCN, are utilized for process optimization (discussed in the following section) and potentially can produce different product(s). For instance, for sacrificial water, it seems methane is the main product and also CO and  $\text{CH}_3\text{OH}$  can produce [1, 45–49]. As another example, for sacrificial methanol, HCOOH and HCHO are expected to be the main products of  $\text{CO}_2$  reduction. It is also plausible that by proceeding the reaction over the time, some of these carbonyl compounds

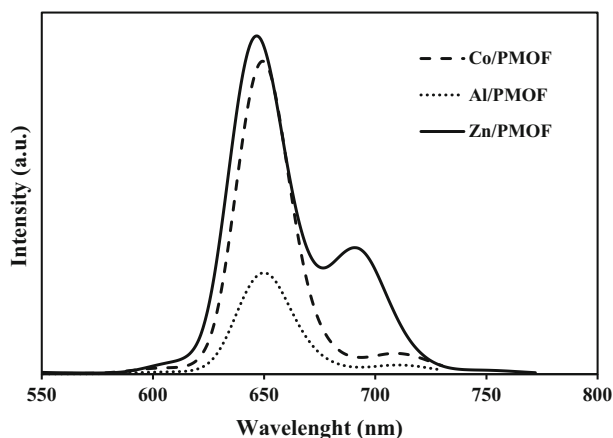


**Fig. 4** Photoluminescence spectra of Zn/PMOF, Al/PMOF and Co/PMOF in DMF solution

mineralized into  $\text{CO}_2$  and  $\text{H}_2\text{O}$ ; and also  $\text{CO}_2$  may undergo methanation by the excited electrons [45, 50, 51]. Consequently, due to the wide variety of the producible products, the  $\text{CO}_2$  conversion was selected as an evaluation measure in the current study.

Fig. 5 demonstrated the photoconversion of  $\text{CO}_2$  under UV/Visible light in the presence of water vapor as electron donor after 4 h. The reaction condition is similar to our previous study [1], 0.3 g of photocatalyst was loaded into the reactor and the pressure of the  $\text{CO}_2$  was 1.4 atm. As it can be seen, the  $\text{CO}_2$  photoconversion obtained by Al/PMOF is 4.3%. Using Zn/PMOF and Co/PMOF as a photocatalyst under similar reaction conditions gave 1.3 and 1.8%, respectively. It can be concluded that the conversion yield obtained by Al/PMOF is about 3.3 and 2.4 times greater than the Zn/PMOF and Co/PMOF, respectively. Overall, the results of these investigations show that Al/PMOF is the best photocatalyst with high  $\text{CO}_2$  photoreduction conversion.

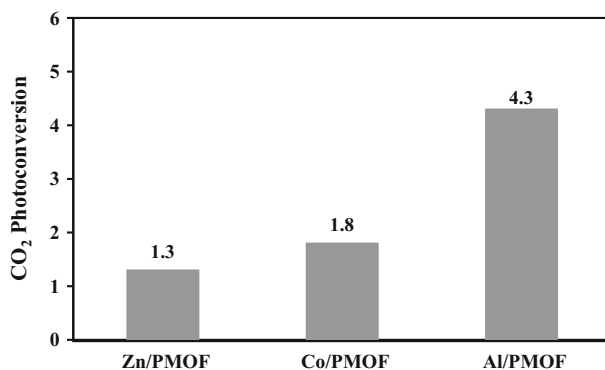


**Fig. 5** Comparison of the  $\text{CO}_2$  photoconversion over Zn/PMOF [1], Al/PMOF and Co/PMOF

In the following, the operating parameters (amount of the catalyst, total pressure of feed and sacrificial agent) are optimized to obtain high CO<sub>2</sub> photoreduction conversion over Al/PMOF.

### Model fitting and statistical analysis

After fitting the obtained data for each parameter of the full second-order model (model containing all two parameter interactions), ANOVA for the model was carried out and the full second-order model significance was examined. Forasmuch as the full second-order model was not fulfilled the determined conditions, it was improved by elimination of model terms.

While using the obtained results, an empirical relationship between the CO<sub>2</sub> photoconversion, response, and the process variables, independent variables, was achieved and expressed by the following second-order polynomial equations for each sacrificial agent:

For H<sub>2</sub>O:

$$\begin{aligned} & \% \text{Photoconversion} \\ & = -1.811 + 0.037273 \times \text{catal.amount} + 1.48395 \\ & \quad \times \text{pressure} - 5.00617 \times 10^{-3} \times \text{catal.amount} \times \text{pressure} \\ & \quad - 5.09048 \times 10^{-5} \times \text{catal.amount}^2 \end{aligned} \quad (4)$$

For MeCN:

$$\begin{aligned} & \% \text{Photoconversion} \\ & = +8.75497 + 0.037273 \times \text{catal.amount} - 1.91235 \\ & \quad \times \text{pressure} - 5.00617 \times 10^{-3} \times \text{catal.amount} \times \text{pressure} \\ & \quad - 5.09048 \times 10^{-5} \times \text{catal.amount}^2 \end{aligned} \quad (5)$$

For methanol:

$$\begin{aligned} & \% \text{Photoconversion} \\ & = +8.50083 + 0.037273 \times \text{catal.amount} - 1.6963 \\ & \quad \times \text{pressure} - 5.00617 \times 10^{-3} \times \text{catal.amount} \times \text{pressure} \\ & \quad - 5.09048 \times 10^{-5} \times \text{catal.amount}^2 \end{aligned} \quad (6)$$

From the ANOVA of the reduced quadratic model (Table 3), the F value for the model is 74.42, which implies that the model is significant. There is only a 0.01% chance that the “model F value” could occur due to noise. Furthermore, the model p-value is < 0.0001, indicating that the model is significant. In this study, the independent variables, including the pressure ( $X_2$ ), sacrificial agent ( $X_3$ ) and interactions between pressure and sacrificial agent ( $X_2X_3$ ) are highly significant parameters with  $p < 0.0001$ . Moreover, the catalyst amount ( $X_1$ ), interactions between catalyst amount and pressure ( $X_1X_2$ ) and the second-order effect of catalyst amount ( $X_1^2$ ) are significant at  $p < 0.05$ . On the other hand, lack of fit of the model is not significant.

**Table 3** ANOVA results for the response surface reduced quadratic model

Source	Sum of squares	Freedom degree	Mean square	F-value	p-value	
Model	202.39	8	25.30	74.42	< 0.0001	Significant
$X_1$ -catalyst amount	1.78	1	1.78	5.23	0.0295	
$X_2$ -pressure	95.80	1	95.80	281.80	< 0.0001	
$X_3$ -sacrificial agent	17.63	2	8.82	25.94	< 0.0001	
$X_1 X_2$	5.50	1	5.50	16.18	0.0004	
$X_2 X_3$	79.17	2	39.58	116.44	< 0.0001	
$X_1^2$	2.51	1	2.51	7.39	0.0108	
Residual	10.20	30	0.34			
Lack of fit	6.91	18	0.38	1.40	0.2798	Not significant
Pure error	3.29	12	0.27			

The important part of the data analysis procedure is the model validity checking. The residual plots were examined by the proposed model. Residuals are the difference between experimental values and the calculated values for each point by the model. Residuals demonstrate how well the model satisfies the assumptions of the ANOVA by detecting some outliers among total data [9, 52, 53]. The normal probability versus studentized residuals plot for CO<sub>2</sub> photoconversion is shown in Fig. S5a (supplementary material). The results in Fig. S5a (supplementary material) indicate the points fall near a straight line which means the residuals follow a normal distribution. Furthermore, the S-shaped curve was not formed in Fig. S5a (supplementary material), indicating that no response transformation was required and also there was not an apparent problem with normality. The plot of studentized residuals versus predicted responses is shown in Fig. S5b (supplementary material). All points of experimental runs are dispersed randomly above and below the horizontal lines between  $\pm 3$ , which confirm the adequacy of the proposed model and also the constant variance assumption was verified [54]. The “pred *R*-squared” of 0.9141 is in reasonable agreement with the “adj *R*-squared” of 0.9392 that confirm good predictability of the model. The accuracy of the model is demonstrated in Fig. S5c (supplementary material), which compares the actual (measured) values against the predicted responses of the model for the CO<sub>2</sub> photoreduction conversion. As observed in Fig. S5c (supplementary material), there are tendencies in the linear regression fit, and the model could be used in the experimental range of studied adequately. The fitted regression equation presented a good fit of the model. Also, the experimental results and the predicted values obtained from the models (Eqs. (4–6)) are presented in Table 2. These results demonstrated good agreements between the experimental and predicted values of CO<sub>2</sub> photoconversion with  $R^2 = 0.9520$ . The correlation coefficient ( $R^2$ ) implies that 95.20% of the variations for percent CO<sub>2</sub> photoconversion are explained by the

independent variables, in other words, this means that the model does not explain only 4.80% of the variation.

### Process optimization and model verification

In this study three-dimensional (3D) and contour (2D) plots were utilized to demonstrate the effect of the one factor on the response value at different levels of other factors. Notably, the 3D plots were obtained based on the proposed model and widely used to realize the interactions between variables within the range considered [54, 55].

Since there was 1 categorical factor ( $X_3$ ) in the experimental design, 3 plots can be determined for each level ( $H_2O$ , MeCN, and methanol). Effects of the interaction between pressure and catalyst amount on the photoreduction conversion of  $CO_2$  are shown in Fig. 6, also, Fig. S6 (supplementary material).

Fig. 6a shows the effects of the pressure and catalyst amount on the  $CO_2$  photoconversion for  $H_2O$  as a sacrificial agent. As can be seen from Fig. 6a, the  $CO_2$  photoconversion percentage increases with increasing pressure. On the other hand, the  $CO_2$  photoconversion decreases with increasing the catalyst amount at the high pressure, 4.1 atm. The influence of pressure on the photoconversion of  $CO_2$  is significant for MeCN as shown in Fig. 6b. Surprisingly, the photoconversion percentage of  $CO_2$  decreases drastically as the pressure increases. It is difficult to explain this result, but it might be related to the deactivation of the photocatalyst surface. There is the tendency toward the accumulation of reaction products on the photocatalyst surface which also resulted in the photocatalyst deactivation after 4 h as reported and discussed in previous studies [1, 2, 5, 56, 57]. Also, this result may be explained by the Le Chatelier's principle. According to this principle, with increasing the system pressure, the reaction favors in the reverse order, and conversion of products to reactants [2, 58, 59]. At low pressure, the  $CO_2$  photoconversion increasing proportionally to the catalyst amount, as expected, confirming the positive influence of the catalyst amount on photocatalytic performance. At high pressure, a slight decrease in  $CO_2$  photoconversion was observed with increasing catalyst amount (from 200 to 300 mg). Similar results were observed for methanol as shown in Fig. 6c.

The main purpose of the experimental design is the optimization of the process which is lead to saving effort, time and process costs that are desirable from industrial standpoint. The program uses several possible goals to conduct desirability indices: maximize, minimize, target, within range, none (for response only) and set to an exact value (factors only). The numerical optimization seeks to maximize the desirability function. Simply put, desirability is an objective function, which ranges from zero outside of the limits to one at the goal, to find the optimum condition [53–55]. In this research, the goal was to reach maximum  $CO_2$  photoconversion. So, all three variables were set at “within range” and the “maximum value” was selected for the response, as shown in Table 4. The result of the optimization is presented in Table 5. From Table 5, the result of the desirability showed that the proposed model equations could adequately be used to describe the  $CO_2$  photoconversion. According to the possible reasons discussed above and also

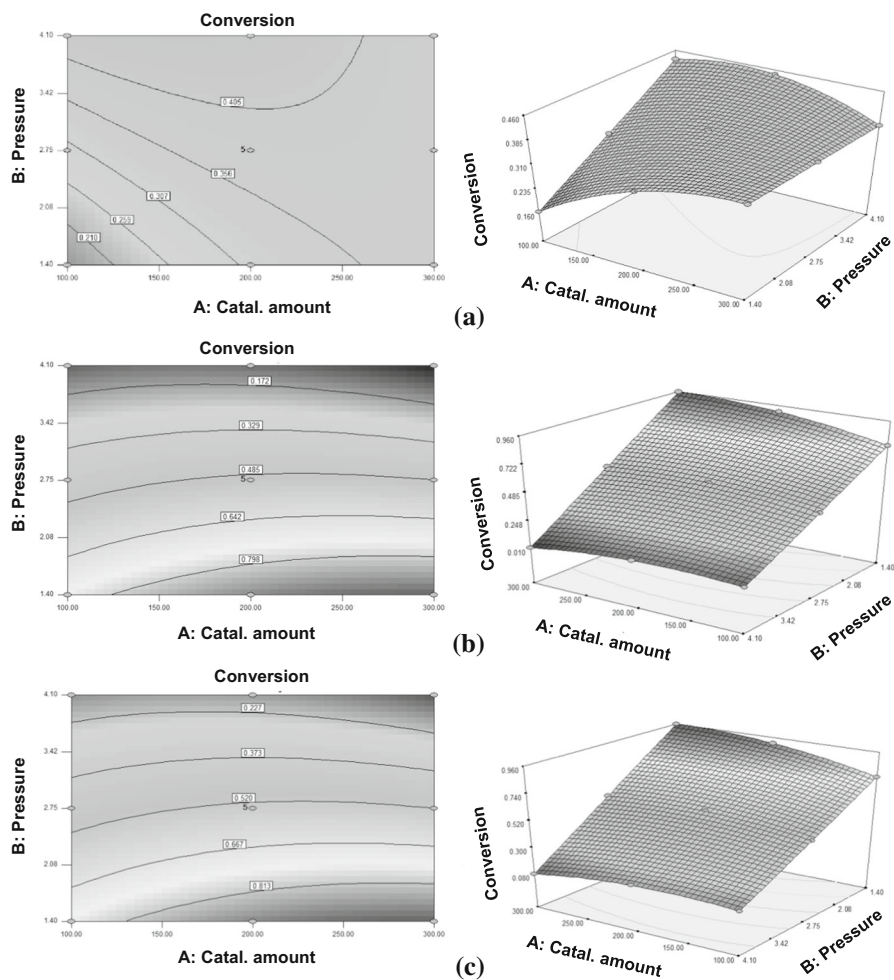


**Fig. 6** The response surface and contour plots of CO<sub>2</sub> photoconversion (%) over Al/PMOF as the function of pressure (atm) and catalyst amount (mg) for **a** H<sub>2</sub>O, **b** MeCN and **c** Methanol as a sacrificial agent

shown in Table 5, the optimum pressure 1.4 atm was found to be having the highest efficiency under the studied experimental conditions. Also, as shown in Table 5 the best sacrificial agent is methanol. This result can be explained by the fact that the  $pK_a$  value of methanol, water and MeCN are 15.5, 15.7 and 25, respectively [60, 61]. It is worthy to note that  $pK_a$  values are a convenient way to compare acid strengths, base strengths, Gibbs free energy changes, etc. The low  $pK_a$  values point to stronger acids while high  $pK_a$  values indicate weak acids [62, 63]. So, it can be concluded that methanol has the lowest  $pK_a$ , so it is more acidity than the other sacrificial agents (MeCN and water).

Besides this matter, for methanol and methoxide anion, the primary interaction (I, Fig. 7) takes place between a filled lone-pair orbital (n) on oxygen and an

**Table 4** Optimization of the individual responses ( $d_i$ ) to obtain the overall desirability response ( $D$ )

Name	Goal	Lower limit	Upper limit	Lower weight	Upper weight	Importance
Catal. amount	In the range	100	300	1	1	3
Pressure	In the range	1.4	4.1	1	1	3
Solvent	In the range	H <sub>2</sub> O	Methanol	1	1	3
Photoconversion	Maximize	1.2	11.02	1	1	3

**Table 5** Comparison between optimized CO<sub>2</sub> photoconversion calculated from central composite design and experimental study

	Catalyst amount (mg)	Pressure (atm)	Sacrificial agent	Photoconversion (%)	Desirability
Optimized CO <sub>2</sub> photoconversion calculated from CCD (predicted value)	297.24	1.4	Methanol	10.63	0.96
Confirmation study of optimized CO <sub>2</sub> photoconversion (experimental value)	297	1.4	Methanol	10.98	
Error(%) = $\frac{\text{Experimental value} - \text{Predicted value}}{\text{Experimental value}} \times 100$				3.18	

unoccupied  $\pi_{Me}^*$  orbital of the methyl group leading to a two-electron stabilizing effect. Deprotonation of OH (giving rise to O<sup>-</sup>) results in an increase in the energy of the n orbitals on oxygen and a declined energy separation between the interacting orbitals n and  $\pi_{Me}^*$  and thus a greater stabilizing interaction (II, Fig. 7). Therefore methyl is more effective in stabilizing the OH<sup>-</sup> anion in comparison with the neutral water molecule, and as a result, methanol is more acidic (in the gas phase) than water [64].

In order to validate the optimum point generated by CCD, an experimental run was performed at the optimum conditions. As shown in Table 5, the experimental value (CO<sub>2</sub> photoconversion: 10.98%) was found to be in good agreement with the predicted value (CO<sub>2</sub> photoconversion: 10.63%). Furthermore, two blank tests were performed: (1) empty reactor (2) catalyst loaded in the reactor in the dark, under same experimental condition. No CO<sub>2</sub> conversion was observed in blank tests. For case (1) no matter the light was on or off. These blank tests prove that the conversion only occurred when catalyst present together with light irradiation. In other words, it can be concluded that the reaction is photocatalytic. Also, The TiO<sub>2</sub> was applied as photocatalyst at the optimum condition for photocatalytic reduction

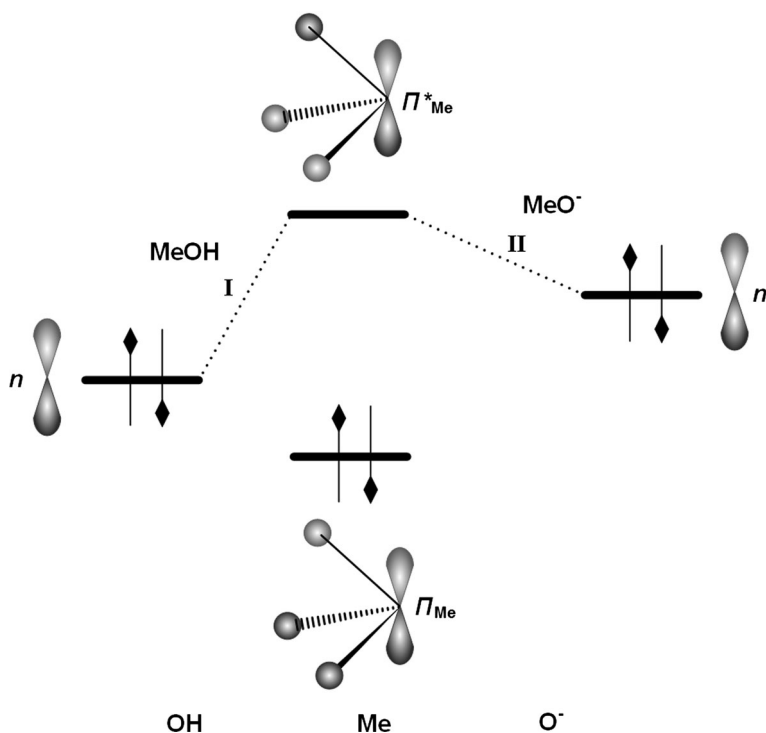


**Fig. 7** Energy diagram demonstrating the interaction of  $\pi_{\text{Me}}$  and  $\pi_{\text{Me}}^*$  orbitals of methyl with a lone-pair orbital (n) of the OH and O<sup>-</sup> groups

of CO<sub>2</sub>. After 4 h illumination, the obtained CO<sub>2</sub> photoconversion was 3.4% where is about 3.3 times less than Al/PMOF. Based on the results, it can conclude that Al/PMOF demonstrates the superiority photocatalytic activity toward CO<sub>2</sub> photoreduction.

## Conclusion

The photocatalytic reduction of CO<sub>2</sub> over M/PMOF under UV/Visible light irradiation was investigated and optimized in this study. In this respect, at first, three different metals (Zn, Al and Co) were used to prepare M/PMOF. According to their photoluminescent properties and photoreactor tests, it was found that Al/PMOF has high CO<sub>2</sub> photoreduction conversion among other two metals (Zn and Co). The second aim of this study was to optimize the operating conditions which mainly influence the photocatalytic reduction of CO<sub>2</sub> as the crucial factor in this process commercialization. Since different employed solvents were used for process optimization and wide variety of different products may be produced, only on the CO<sub>2</sub> photoconversion was selected as an evaluation measure of the process. Analysis of variance results for the reduced quadratic model demonstrated a high

coefficient determination ( $R^2 = 0.9520$  and  $\text{Adj-}R^2 = 0.9392$ ), thus ensuring a satisfactory adjustment of the second-order regression model with the experimental data. Optimizing experimental conditions showed that the maximum photoconversion of  $\text{CO}_2$  was achieved in catalyst amount of 297.24 mg, total feed pressure of 1.4 atm and methanol as a sacrificial agent. Under optimized condition, the experimentally measured value of  $\text{CO}_2$  photocatalytic reduction was in good agreement with the predicted value implied that the optimization using RSM based on central composite design can save time and effort by the estimation of the optimum conditions of the maximum photoreduction conversion of  $\text{CO}_2$ .

**Acknowledgements** This work was partly supported by the Natural Science and Engineering Research Council of Canada (NSERC) through the Discovery Grant. The authors are deeply appreciated Professor Trong-On DO for his helpful comments. A portion of this work was performed in his laboratory.

## References

1. Sadeghi N, Sharifnia S, Sheikh Arabi M (2016) A porphyrin-based metal organic framework for high rate photoreduction of  $\text{CO}_2$  to  $\text{CH}_4$  in gas phase. *J CO<sub>2</sub> Util* 16:450–457. <https://doi.org/10.1016/j.jcou.2016.10.006>
2. Torabi Merajin M, Sharifnia S, Mansouri AM (2014) Process modeling and optimization of simultaneous direct conversion of  $\text{CO}_2$  and  $\text{CH}_4$  greenhouse gas mixture over  $\text{TiO}_2/\text{webnet}$  photocatalyst. *J Taiwan Inst Chem Eng* 45(3):869–879. <https://doi.org/10.1016/j.jtice.2013.09.013>
3. Gharaié M, Zhang N, Jobson M, Smith R, Panjeshahi MH (2013) Simultaneous optimization of  $\text{CO}_2$  emissions reduction strategies for effective carbon control in the process industries. *Chem Eng Res Des* 91(8):1483–1498. <https://doi.org/10.1016/j.cherd.2013.06.006>
4. Sakkas VA, Islam MA, Stalikas C, Albanis TA (2010) Photocatalytic degradation using design of experiments: a review and example of the Congo red degradation. *J Hazard Mater* 175(1–3):33–44. <https://doi.org/10.1016/j.jhazmat.2009.10.050>
5. Akhter P, Hussain M, Saracco G, Russo N (2015) Novel nanostructured- $\text{TiO}_2$  materials for the photocatalytic reduction of  $\text{CO}_2$  greenhouse gas to hydrocarbons and syngas. *Fuel* 149:55–65. <https://doi.org/10.1016/j.fuel.2014.09.079>
6. Baş D, Boyacı İH (2007) Modeling and optimization I: usability of response surface methodology. *J Food Eng* 78(3):836–845. <https://doi.org/10.1016/j.jfoodeng.2005.11.024>
7. Bezerra MA, Santelli RE, Oliveira EP, Villar LS, Escalera LA (2008) Response surface methodology (RSM) as a tool for optimization in analytical chemistry. *Talanta* 76(5):965–977. <https://doi.org/10.1016/j.talanta.2008.05.019>
8. Ansari F, Ghaedi M, Taghdiri M, Asfaram A (2016) Application of ZnO nanorods loaded on activated carbon for ultrasonic assisted dyes removal: experimental design and derivative spectrophotometry method. *Ultrason Sonochem* 33:197–209. <https://doi.org/10.1016/j.ultsonch.2016.05.004>
9. Amdoun R, Khelifi L, Khelifi-Slaoui M, Amroune S, Asch M, Assaf-Ducrocq C, Gontier E (2010) Optimization of the culture medium composition to improve the production of hyoscyamine in elicited *Datura stramonium* L. hairy roots using the response surface methodology (RSM). *Int J Mol Sci*. <https://doi.org/10.3390/ijms11114726>
10. Desai KM, Vaidya BK, Singhal RS, Bhagwat SS (2005) Use of an artificial neural network in modeling yeast biomass and yield of  $\beta$ -glucan. *Process Biochem* 40(5):1617–1626. <https://doi.org/10.1016/j.procbio.2004.06.015>
11. Mjalli FS, Al-Asheh S, Alfadala HE (2007) Use of artificial neural network black-box modeling for the prediction of wastewater treatment plants performance. *J Environ Manage* 83(3):329–338. <https://doi.org/10.1016/j.jenvman.2006.03.004>
12. Dreiseitl S, Ohno-Machado L (2002) Logistic regression and artificial neural network classification models: a methodology review. *J Biomed Inform* 35(5–6):352–359. [https://doi.org/10.1016/S1532-0464\(03\)00034-0](https://doi.org/10.1016/S1532-0464(03)00034-0)

13. Tu JV (1996) Advantages and disadvantages of using artificial neural networks versus logistic regression for predicting medical outcomes. *J Clin Epidemiol* 49(11):1225–1231. [https://doi.org/10.1016/S0895-4356\(96\)00002-9](https://doi.org/10.1016/S0895-4356(96)00002-9)
14. Ciprian-George Piuleac CS, Cañizares Pablo, Curteanu Silvia, Rodrigo Manuel Andrés (2012) Hybrid model of a wastewater-treatment electrolytic process. *Int J Electrochem Sci* 7(7):6289–6301
15. Pal MP, Vaidya BK, Desai KM, Joshi RM, Nene SN, Kulkarni BD (2009) Media optimization for biosurfactant production by *Rhodococcus erythropolis* MTCC 2794: artificial intelligence versus a statistical approach. *J Ind Microbiol Biotechnol* 36(5):747–756. <https://doi.org/10.1007/s10295-009-0547-6>
16. Curteanu S, Piuleac CG, Godini K, Azaryan G (2011) Modeling of electrolysis process in wastewater treatment using different types of neural networks. *Chem Eng J* 172(1):267–276. <https://doi.org/10.1016/j.cej.2011.05.104>
17. Oliveira R, Almeida MF, Santos L, Madeira LM (2006) Experimental design of 2,4-dichlorophenol oxidation by Fenton's reaction. *Int J Electrochem Sci* 45(4):1266–1276. <https://doi.org/10.1021/ie0509544>
18. Mosleh S, Rahimi MR, Ghaedi M, Dashtian K, Hajati S (2016) Photocatalytic degradation of binary mixture of toxic dyes by HKUST-1 MOF and HKUST-1-SBA-15 in a rotating packed bed reactor under blue LED illumination: central composite design optimization. *RSC Adv* 6(21):17204–17214. <https://doi.org/10.1039/c5ra24564h>
19. Ahmadi M, Vahabzadeh F, Bonakdarpour B, Mofarrah E, Mehranian M (2005) Application of the central composite design and response surface methodology to the advanced treatment of olive oil processing wastewater using Fenton's peroxidation. *J Hazard Mater* 123(1–3):187–195. <https://doi.org/10.1016/j.jhazmat.2005.03.042>
20. Mahmodi G, Sharifnia S, Rahimpour F, Hosseini SN (2013) Photocatalytic conversion of CO<sub>2</sub> and CH<sub>4</sub> using ZnO coated mesh: effect of operational parameters and optimization. *Sol Energ Mat Sol Cells* 111:31–40. <https://doi.org/10.1016/j.solmat.2012.12.017>
21. Sasikumar E, Viruthagiri T (2008) Optimization of process conditions using response surface methodology (RSM) for ethanol production from pretreated sugarcane Bagasse: kinetics and modeling. *Bio Energy Res* 1(3):239–247. <https://doi.org/10.1007/s12155-008-9018-6>
22. Zhang H, Li Y, Lu Z, Wu M, Shi R, Chen L (2017) Highly efficient synthesis of biodiesel catalyzed by CF<sub>3</sub>SO<sub>3</sub>H-functionalized ionic liquids: experimental design and study with response surface methodology. *React Kinet Mech Catal* 121(2):579–592. <https://doi.org/10.1007/s11144-017-1171-5>
23. Baziari A, Ghashang M (2016) Preparation of pyrano[3,2-c]chromene-3-carbonitriles using ZnO nano-particles: a comparison between the Box-Behnken experimental design and traditional optimization methods. *React Kinet Mech Catal* 118(2):463–479. <https://doi.org/10.1007/s11144-016-1013-x>
24. Montgomery DC, Runger GC, Hubele NF (2001) *Engineering statistics*. Wiley, New Jersey
25. Vining GG (2003) *Statistical methods for engineers*, 3rd edn. Cengage Learning, Boston
26. Parajó JC, Alonso JL, Lage MA, Vázquez D (1992) Empirical modeling of eucalyptus wood processing. *Bioprocess Eng* 8(3):129–136. <https://doi.org/10.1007/bf01254228>
27. Wen Z, Liao W, Chen S (2005) Production of cellulase by *Trichoderma reesei* from dairy manure. *Bioresour Technol* 96(4):491–499. <https://doi.org/10.1016/j.biortech.2004.05.021>
28. Beg QK, Sahai V, Gupta R (2003) Statistical media optimization and alkaline protease production from *Bacillus mojavensis* in a bioreactor. *Process Biochem* 39(2):203–209. [https://doi.org/10.1016/S0032-9592\(03\)00064-5](https://doi.org/10.1016/S0032-9592(03)00064-5)
29. Mayerhoff ZDVL, Roberto IC, Franco TT (2004) Purification of xylose reductase from *Candida mogii* in aqueous two-phase systems. *Biochem Eng J* 18(3):217–223. <https://doi.org/10.1016/j.bej.2003.09.003>
30. Muthukumar M, Sargunamani D, Selvakumar N, Venkata Rao J (2004) Optimisation of ozone treatment for colour and COD removal of acid dye effluent using central composite design experiment. *Dyes Pigment* 63(2):127–134. <https://doi.org/10.1016/j.dyepig.2004.02.003>
31. Mosleh S, Rahimi MR, Ghaedi M, Dashtian K, Hajati S (2016) BiPO<sub>4</sub>/Bi<sub>2</sub>S<sub>3</sub>-HKUST-1-MOF as a novel blue light-driven photocatalyst for simultaneous degradation of toluidine blue and auramine-O dyes in a new rotating packed bed reactor: optimization and comparison to a conventional reactor. *RSC Adv* 6(68):63667–63680. <https://doi.org/10.1039/c6ra10385e>
32. Mosleh S, Rahimi MR, Ghaedi M, Dashtian K (2016) Sonophotocatalytic degradation of trypan blue and vesuvine dyes in the presence of blue light active photocatalyst of Ag<sub>3</sub>PO<sub>4</sub>/Bi<sub>2</sub>S<sub>3</sub>-HKUST-1-

- MOF: central composite optimization and synergistic effect study. *Ultrason Sonochem* 32:387–397. <https://doi.org/10.1016/j.ultsonch.2016.04.007>
33. Wang C-C, Zhang Y-Q, Li J, Wang P (2015) Photocatalytic CO<sub>2</sub> reduction in metal–organic frameworks: a mini review. *J Mol Struct* 1083:127–136. <https://doi.org/10.1016/j.molstruc.2014.11.036>
  34. Ryder MR, Tan J-C (2014) Nanoporous metal organic framework materials for smart applications. *Mater Sci Technol* 30(13a):1598–1612. <https://doi.org/10.1179/1743284714Y.0000000550>
  35. Shi L, Wang T, Zhang H, Chang K, Ye J (2015) Electrostatic self-assembly of nanosized carbon nitride nanosheet onto a zirconium metal–organic framework for enhanced photocatalytic CO<sub>2</sub> reduction. *Adv Funct Mater* 25(33):5360–5367. <https://doi.org/10.1002/adfm.201502253>
  36. Wang S, Lin J, Wang X (2014) Semiconductor–redox catalysis promoted by metal–organic frameworks for CO<sub>2</sub> reduction. *Phys Chem Chem Phys* 16(28):14656–14660. <https://doi.org/10.1039/c4cp02173h>
  37. Fateeva A, Chater PA, Ireland CP, Tahir AA, Khimyak YZ, Wiper PV, Darwent JR, Rosseinsky MJ (2012) A water-stable porphyrin-based metal–organic framework active for visible-light photocatalysis. *Angew Chem Int Ed* 51(30):7440–7444. <https://doi.org/10.1002/anie.201202471>
  38. Liu Y, Yang Y, Sun Q, Wang Z, Huang B, Dai Y, Qin X, Zhang X (2013) Chemical adsorption enhanced CO<sub>2</sub> capture and photoreduction over a copper porphyrin based metal organic framework. *ACS Appl Mater Interf* 5(15):7654–7658. <https://doi.org/10.1021/am4019675>
  39. Yuan Y-J, Tu J-R, Ye Z-J, Lu H-W, Ji Z-G, Hu B, Li Y-H, Cao D-P, Yu Z-T, Zou Z-G (2015) Visible-light-driven hydrogen production from water in a noble-metal-free system catalyzed by zinc porphyrin sensitized MoS<sub>2</sub>/ZnO. *Dyes Pigm* 123:285–292. <https://doi.org/10.1016/j.dyepig.2015.08.014>
  40. Yuan Y, Lu H, Ji Z, Zhong J, Ding M, Chen D, Li Y, Tu W, Cao D, Yu Z, Zou Z (2015) Enhanced visible-light-induced hydrogen evolution from water in a noble-metal-free system catalyzed by ZnTCPP-MoS<sub>2</sub>/TiO<sub>2</sub> assembly. *Chem Eng J* 275:8–16. <https://doi.org/10.1016/j.cej.2015.04.015>
  41. Krishna MBM, Venkatramiah N, Venkatesan R, Narayana Rao D (2012) Synthesis and structural, spectroscopic and nonlinear optical measurements of graphene oxide and its composites with metal and metal free porphyrins. *J Mater Chem* 22(7):3059–3068. <https://doi.org/10.1039/c1jm14822b>
  42. Seoudi R, El-Bahy GS, El Sayed ZA (2005) FTIR, TGA and DC electrical conductivity studies of phthalocyanine and its complexes. *J Mol Struct* 753(1):119–126. <https://doi.org/10.1016/j.molstruc.2005.06.003>
  43. Jo SW, Kwak BS, Kim KM, Do JY, Park N-K, Ryu SO, Ryu H-J, Baek J-I, Kang M (2015) Effectively CO<sub>2</sub> photoreduction to CH<sub>4</sub> by the synergistic effects of Ca and Ti on Ca-loaded TiSiMCM-41 mesoporous photocatalytic systems. *Appl Surf Sci* 355:891–901. <https://doi.org/10.1016/j.apsusc.2015.07.176>
  44. Ngo TT (2016) Photocatalytic reduction of CO<sub>2</sub> with tunable bandgap and bandedge materials. University of South Florida, Tampa
  45. Karamian E, Sharifnia S (2016) On the general mechanism of photocatalytic reduction of CO<sub>2</sub>. *J CO<sub>2</sub> Util* 16:194–203. <https://doi.org/10.1016/j.jcou.2016.07.004>
  46. Ji Y, Luo Y (2016) Theoretical study on the mechanism of photoreduction of CO<sub>2</sub> to CH<sub>4</sub> on the anatase TiO<sub>2</sub>(101) surface. *ACS Catal* 6(3):2018–2025. <https://doi.org/10.1021/acscatal.5b02694>
  47. Murcia-Lopez S, Vaiano V, Hidalgo MC, Navio JA, Sannino D (2015) Photocatalytic reduction of CO<sub>2</sub> over platinumised Bi<sub>2</sub>WO<sub>6</sub>-based materials. *Photochem Photobiol Sci* 14(4):678–685. <https://doi.org/10.1039/c4pp00407h>
  48. Fresno F, Jana P, Renones P, Coronado JM, Serrano DP, de la Pena O'Shea VA (2017) CO<sub>2</sub> reduction over NaNbO<sub>3</sub> and NaTaO<sub>3</sub> perovskite photocatalysts. *Photochem Photobiol Sci* 16(1):17–23. <https://doi.org/10.1039/c6pp00235h>
  49. Zhou S-S, Liu S-Q (2017) Photocatalytic reduction of CO<sub>2</sub> based on a CeO<sub>2</sub> photocatalyst loaded with imidazole fabricated N-doped graphene and Cu(ii) as cocatalysts. *Photochem Photobiol Sci* 16(10):1563–1569. <https://doi.org/10.1039/c7pp00211d>
  50. Chen J, Xin F, Qin S, Yin X (2013) Photocatalytically reducing CO<sub>2</sub> to methyl formate in methanol over ZnS and Ni-doped ZnS photocatalysts. *Chem Eng J* 230:506–512. <https://doi.org/10.1016/j.cej.2013.06.119>
  51. Dey GR, Pushpa KK (2006) Methane generated during photocatalytic redox reaction of alcohols on TiO<sub>2</sub> suspension in aqueous solutions. *Res Chem Intermediat* 32(8):725–736. <https://doi.org/10.1163/156856706778606462>

52. Körbahti BK, Rauf MA (2008) Response surface methodology (RSM) analysis of photoinduced decoloration of toluidine blue. *Chem Eng J* 136(1):25–30. <https://doi.org/10.1016/j.cej.2007.03.007>
53. Shahrezaei F, Mansouri Y, Zinatizadeh AAL, Akhbari A (2012) Process modeling and kinetic evaluation of petroleum refinery wastewater treatment in a photocatalytic reactor using TiO<sub>2</sub> nanoparticles. *Powder Technol* 221:203–212. <https://doi.org/10.1016/j.powtec.2012.01.003>
54. Yaqubzadeh AR, Ahmadpour A, Bastami TR, Hataminia MR (2016) Low-cost preparation of silica aerogel for optimized adsorptive removal of naphthalene from aqueous solution with central composite design (CCD). *J Non-Cryst Solid* 447:307–314. <https://doi.org/10.1016/j.jnoncrsol.2016.06.022>
55. Vaez M, Zarringhalam Moghaddam A, Alijani S (2012) Optimization and modeling of photocatalytic degradation of Azo dye using a response surface methodology (RSM) based on the central composite design with immobilized titania nanoparticles. *Ind Eng Chem Res* 51(11):4199–4207. <https://doi.org/10.1021/ie202809w>
56. Sasirekha N, Basha SJS, Shanthy K (2006) Photocatalytic performance of Ru doped anatase mounted on silica for reduction of carbon dioxide. *Appl Catal B* 62(1–2):169–180. <https://doi.org/10.1016/j.apcatb.2005.07.009>
57. Ahmad Beigi A, Fatemi S, Salehi Z (2014) Synthesis of nanocomposite CdS/TiO<sub>2</sub> and investigation of its photocatalytic activity for CO<sub>2</sub> reduction to CO and CH<sub>4</sub> under visible light irradiation. *J CO<sub>2</sub> Util* 7:23–29. <https://doi.org/10.1016/j.jcou.2014.06.003>
58. Joos P, Serrien G (1991) The principle of Braun—Le Châtelier at surfaces. *J Colloid Interf Sci*. 145(1):291–294. [https://doi.org/10.1016/0021-9797\(91\)90123-P](https://doi.org/10.1016/0021-9797(91)90123-P)
59. Jenkins HDB (2008) Le Chatelier's Principle. *Chemical Thermodynamics at a Glance*. Blackwell Publishing Ltd, New Jersey, pp 160–163. <https://doi.org/10.1002/9780470697733.ch49>
60. Brown W, Foote C, Iverson B, Anslyn E (2008) *Organic chemistry*. Cengage Learning, Boston
61. van Gunsteren WF, Weiner PK, Wilkinson T, Wilkinson AJ (1997) *Computer simulation of biomolecular systems: theoretical and experimental applications*. Springer, New York
62. Shields GC, Seybold PG (2013) *Computational approaches for the prediction of pKa values*. CRC Press, Boca Raton
63. Menger FM (1980) *Electronic interpretation of organic chemistry: a problems-oriented text*. Springer, New York
64. Pross A, Radom L (1978) Does a methyl substituent stabilize or destabilize anions? *Am Chem Soc* 100(21):6572–6575. <https://doi.org/10.1021/ja00489a005>